

Removal and mixing of the coronal gas from satellites in galaxy groups: cooling the intragroup gas

Jesús Zavala^{1,2*}, Michael L. Balogh¹, Niayesh Afshordi^{2,1} and Stephen Ro¹

¹*Department of Physics and Astronomy, University of Waterloo, Waterloo, Ontario, N2L 3G1, Canada*

²*Perimeter Institute for Theoretical Physics, 31 Caroline St. N., Waterloo, ON, N2L 2Y5, Canada*

27 August 2012

ABSTRACT

The existence of an extended hot gaseous corona surrounding clusters, groups and massive galaxies is well established by observational evidence and predicted by current theories of galaxy formation. When a small galaxy collides with a larger one, their coronae are the first to interact, producing disturbances that remove gas from the smaller system and settle it into the corona of the larger one. For a Milky-Way-size galaxy merging into a low-mass group, ram pressure stripping and the Kelvin-Helmholtz instability are the most relevant of these disturbances. We argue that the turbulence generated by the latter mixes the material of both coronae in the wake of the orbiting satellite creating a “warm phase” mixture with a cooling time a factor of several shorter than that of the ambient intragroup gas. We reach this conclusion using analytic estimates, as well as adiabatic and dissipative high resolution numerical simulations of a spherical corona subject to the ablation process of a constant velocity wind with uniform density and temperature. Although this is a preliminary analysis, our results are promising and we speculate that the mixture could potentially trigger in situ star formation and/or be accreted into the central galaxy as a cold gas flow resulting in a new mode of star formation in galaxy groups and clusters.

Key words: hydrodynamics - turbulence - cooling flows - galaxies: evolution - groups - interaction - methods: analytical - numerical

1 INTRODUCTION

The classical theory of galaxy formation establishes that gas follows dark matter in its non-linear evolution as it forms virialized dark matter haloes. In this process, the gas is heated by shocks and adiabatic compression, acquiring the virial temperature of the halo it has fallen into (White & Rees 1978). Afterwards, the gas can lose energy effectively through radiative cooling if the cooling time is much smaller than the free-fall time ($t_{\text{cool}} < t_{\text{ff}}$), producing a contraction of the gas towards the centre: a cooling flow that fuels star formation. The critical mass for effective cooling depends on the density, temperature and metallicity of the gas. Assuming constant gas density and temperature, one can show that the gas in haloes with primordial gas masses $\gtrsim 10^{11} M_{\odot}$ cannot cool effectively (e.g. see Fig. 8.6 of Mo et al. 2010); this is why galaxy groups and clusters are expected to have a corona of hot gas at the present time.

X-ray observations of relaxed clusters and groups show indeed the presence of an extended gas corona within the

intra-cluster and intra-group medium (hereafter called ICM in both cases), which is approximately in hydrostatic equilibrium within the gravitational potential of the cluster/group. For the most massive systems, the density profile of this diffuse gas approximately traces that of the predicted dark matter distribution (e.g. Vikhlinin et al. 2006). Since the dominant cooling channel in these systems is bremsstrahlung radiation, then $t_{\text{cool}} \propto T^{1/2} \rho^{-1}$ (for primordial composition) which implies that the cooling time scales are typically shorter in the central regions, and hence, in the absence of a balancing heat source, a cooling flow would develop in the centre. Close to the virial radius of the system however, the typical cooling times are larger than the Hubble time.

A hot extended corona is also predicted to exist within the haloes of massive galaxies, including those at the scale of the Milky-Way (MW; White & Frenk 1991). In the absence of additional energy sources, and under idealized circumstances, the majority of this gas would be expected to cool and collapse into the halo centre over a Hubble time; in contrast, roughly 20% of the expected baryons in these haloes are observed to be in a cold phase (stars and cold gas, see e.g. Fukugita & Peebles 2004, 2006, and references

* CITA National Fellow, e-mail: jzavalaf@uwaterloo.ca

therein). This overcooling problem can be avoided by invoking feedback processes that prevent the gas from cooling catastrophically. Recent cosmological simulations that include radiative cooling, star formation and feedback predict that MW-size haloes should have a gas corona surviving today in quasi-hydrostatic equilibrium (e.g. Crain et al. 2010; van de Voort & Schaye 2012). It has also been argued that even without feedback, the combined effect of buoyancy and thermal conduction suppresses the thermal instability, and thus the formation of cold clouds, in stratified coronae in MW-size galaxies (Binney et al. 2009; Nipoti 2010).

The presence of extended coronae has been confirmed for elliptical galaxies through X-ray observations (see review by Mathews & Brighenti 2003) but the evidence for MW-like galaxies is not conclusive. Recent observations have detected diffuse X-ray emission around disc-dominated galaxies, but is approximately two orders of magnitude lower than the expectations based on the White & Frenk (1991) model (e.g. Li et al. 2007); supernovae heating is advocated as the likely cause of this discrepancy (e.g. Crain et al. 2010; Anderson & Bregman 2011; Dai et al. 2012). We note that although there is evidence for the presence of gaseous coronae around galaxies, their cosmological origin as a shock-heated remnant is not settled. There are other possible origins such as enriched gas produced by galactic stellar feedback (e.g. Ciotti & Ostriker 1997; Mathews & Brighenti 1998).

It is thus relevant to consider in detail the impact of the gaseous coronae on the process of galaxy formation, particularly during galaxy mergers. In these events, the gas in the merging galaxies is subject to different processes that remove gas from the satellite: i) ram pressure stripping removes the most loosely bound material (Gunn & Gott 1972) creating a wake that trails behind the satellite (recent observations show evidence of such wakes in galaxies falling into clusters, e.g. Sun et al. 2010, but the stripped gas in the observed cases is the cold ISM of the galaxy, not its corona); ii) thermal conduction causes evaporation of the colder gas in the satellite (Cowie & McKee 1977); iii) if the flow around the boundary interface is laminar then viscosity will cause a drag that will remove gas (Nulsen 1982); iv) fluid instabilities such as the Kelvin-Helmholtz (KH) instability caused by the velocity shear between the layer interface also lead to gas removal.

All these processes have been studied in the past and for the case of galaxies merging into clusters, particular attention has been given to ram pressure stripping using analytic and numerical methods (Mori & Burkert 2000; Heinz et al. 2003; McCarthy et al. 2008). Most of these studies focus on the impact of the removal of gas in the star formation efficiency of the satellite: by completely stripping the gas corona, a fuel reservoir is removed, resulting in a quenching of star formation relative to a case where the galaxy evolves in isolation (this process is usually called “strangulation”). Recent analyses show that a substantial fraction of the corona can actually survive if the satellite is massive enough, and through subsequent radiative cooling, can contribute to star formation (McCarthy et al. 2008; Moster et al. 2011).

The fate of the stripped gas has not been analysed in detail however. As mentioned before, the gas from the satellite removed by ram pressure will form an elongated wake trailing the satellite. Due to the gravity of the satellite, a

similar wake will be formed with gas from the ICM that gets gravitationally focused (Stevens et al. 1999; Sakellou 2000). Thus, in general we would expect a wake composed of material from both the ICM and the corona of the satellite, implying that both gaseous components mix during the removal processes. This mixing is particularly efficient during the turbulence caused by KH instabilities. If the gas removal rate is large and the mixing process is efficient then the mixture will have a temperature that might be significantly lower than the temperature of the ICM. This would imply that the cooling time in the wake is lower than that in the ambient medium, making the mixture a potential fuel source for star formation. This idea has been proposed recently by Marinacci et al. (2010) in the context of a mode of gas accretion triggered by the interaction of H_1 clouds expelled from galactic discs in a galactic fountain, and the corona of the galaxy (see also Heitsch & Putman 2009). In this paper we argue that the same mechanism is at play when the coronae of the merging galaxies interact.

Most of the hydrodynamical simulations of galaxy formation carried out to date have used the smoothed particle hydrodynamics (SPH) technique (for a review see Springel 2010b). This is a formulation that has excellent conservation properties in terms of mass, energy, momentum and entropy and it is fully Galilean invariant. However, SPH considerably suppresses the formation of turbulence triggered by instabilities and thus it is not able to account for gas mixing (Agertz et al. 2007; Bauer & Springel 2012). Adaptive Mesh Refinement (AMR) codes based on an Eulerian formulation are the other method currently used for simulations of galaxy formation. Although they suffer their own shortcomings (like the lack of Galilean invariance), perhaps the most important difference with SPH methods is precisely that of the treatment of turbulence and mixing (Mitchell et al. 2009), which are not suppressed in AMR.

In this paper we take a first step in investigating the effect of mixing in the interaction of coronae in galaxy mergers, focusing on the formation of the trailing wake. For this purpose we start by revisiting analytically the most important gas removal processes and estimate the properties of the resultant gas mixture (Section 2). We then verify these estimates using 3D adiabatic (non-radiative), as well as dissipative simulations of the motion of a spherical corona through a constant density ICM using the AMR code FLASH (Section 3). Our results are presented in Section 4 and finally a discussion and our conclusions are given in Sections 5 and 6. Although our simulations lack several important physical processes that could impact the results, our objective here is to make an initial assessment of whether or not the removed coronal gas could continue to be a source of star formation.

2 THEORETICAL EXPECTATIONS

In this section, we present analytic estimates of what might happen to the gas in the corona of a satellite as it merges with that of a group/cluster. The corona is embedded in a spherical dark matter halo which is assumed to have a radial density distribution given by the Navarro-Frenk-White

Table 1. Typical values for the global properties of a MW-size galaxy, a low-mass group and a cluster.

System	$M_v(M_\odot)$	$r_v(\text{kpc})$	$V_v(\text{km/s})$	$T_v(\text{K})$	$c_s(\text{km/s})^a$
MW-size galaxy	10^{12}	200	146	7.7×10^5	135
low-mass group	10^{13}	430	315	3.6×10^6	291
cluster	10^{14}	931	680	1.7×10^7	627

^a The local sound speed is given by $c_s^2 = \gamma P / \rho$ with $\gamma = 5/3$.

(NFW) profile (Navarro et al. 1996, 1997)¹, which in terms of the dimensionless variable $s = r/r_v$, where r_v is the virial radius, can be written as:

$$\rho(s) = \frac{\rho_{\text{crit}} \delta_c}{cs(1+cs)^2}, \quad (1)$$

where c is the concentration parameter, ρ_{crit} is the critical density and δ_c is a function of the concentration:

$$\delta_c = \frac{\Delta}{3} \frac{c^3}{\log(1+c) - c/(1+c)}. \quad (2)$$

The virial radius r_v is defined as the radius where the mean density of the halo is equal to Δ times the critical density: $M_v/(4\pi r_v^3/3) = \Delta \rho_{\text{crit}}$, where M_v is the total mass within r_v . The value of the density contrast Δ is conventional and varies in the literature, but we use $\Delta = 200$ for this work. The concentration correlates strongly with virial mass and redshift (e.g. Gao et al. 2008). When a numerical value is needed, we adopt the mass-concentration relation found in Neto et al. (2007) based on the Millennium simulation of structure formation (Springel et al. 2005).

We further assume that the dark matter haloes contain a distribution of gas that also follows the NFW profile but normalised by the universal fraction of baryons to dark matter $f_b = \Omega_b/(\Omega_m - \Omega_b)$. Whenever it is needed, we take $\Omega_m = 0.25$ and $\Omega_b = 0.045$ as the values for the contributions from matter and baryons to the total energy density of the Universe, respectively.

The pressure profile is obtained by assuming that the coronal gas is in hydrostatic equilibrium:

$$\frac{dP}{ds} = -\rho_{\text{gas}} \frac{d\phi}{ds}, \quad (3)$$

where $\phi(s)$ is the total gravitational potential (dark matter + gas). To obtain a boundary condition for Eq. (3), we note that the virial velocity of the dark matter halo $V_v^2 = GM_v/r_v$ determines a characteristic temperature for the corona $T_v = \mu m_H V_v^2 / (2k_B)$, where μ is the mean molecular weight of the gas ($\mu^{-1} = 1.71$ for gas with primordial composition), m_H is the mass of a hydrogen atom and k_B is the Boltzmann constant. This characteristic value, and also the assumption of hydrostatic equilibrium, are motivated by the formation of the corona when the gas fell into the halo and got shock-heated to temperatures of the order of T_v . The boundary condition for Eq. (3) is then set by P_v given by the

value of the virial temperature of the halo and the equation of state (EoS), assumed to be that of an ideal gas. Since T_v is actually close to the peak of the temperature profile, we apply a small correction (a factor of $\sim 3/4$) to the value of P_v to obtain a temperature profile that decays as a power law at large radii, which is a behaviour seen in observations of nearby galaxy clusters and groups (e.g. Vikhlinin et al. 2005), as well as in full hydrodynamical simulations of such systems (e.g. Borgani et al. 2004).

Unless otherwise stated, we assume that the satellite halo enters the ICM with a relative velocity v_{sat} which is of the order of the virial velocity of the host $V_{v,\text{host}}$. Throughout this section, we compare the relevance of different processes during the interaction of the hot coronae in two cases: a MW-size galaxy falling into a low-mass group (galaxy-group collision) and the same galaxy falling into a cluster (galaxy-cluster collision). The merger mass ratio in the cases of interest is ≤ 10 , so the gravitational potential of the most massive system is not significantly affected. The characteristic parameters of these three systems appear in Table 1.

2.1 Removal of gas from the satellite

2.1.1 Ram Pressure Stripping (RPS)

As the satellite moves through the ICM, the ram pressure ($P_{\text{ram}} \equiv \rho_{\text{host}} v_{\text{sat}}^2$) imparted to its corona will be sufficient to remove gas from the satellite if it can overcome its gravitational restoring force per unit area (McCarthy et al. 2008, based on Gunn & Gott 1972):

$$P_{\text{ram}} > \alpha_g \frac{G m_{\text{tot}}(< r) \rho_{\text{sat}}(r)}{r}, \quad (4)$$

where $\rho_{\text{sat}}(r)$ is the gas density profile of the corona of the satellite, $m_{\text{tot}}(< r)$ its total mass profile (dark matter + gas), and α_g is a geometric factor of $\mathcal{O}(1)$ depending on the total mass and gas density profiles of the satellite; for instance, $\alpha_g = \pi/2$ for a singular isothermal sphere. The radius where the lhs and rhs of Eq. (4) are equal is the predicted radius r_{rps} that the gas sphere will have after stripping; $m_{\text{sat}}(< r_{\text{rps}})$ is then the surviving mass.

As long as the relative velocity between both systems is supersonic, the collision drives a shock that propagates through the satellite; otherwise a compression wave is formed that propagates with the local sound speed. It is possible to estimate the speed of this shock and its subsequent propagation as a function of the radius of the satellite $v_{\text{sh}}(r)$ by solving a one-dimensional shock tube problem, neglecting the effects of gravity (see Appendix A). The characteristic RPS time scale is then roughly given by the time

¹ The most recent N-body simulations of structure formation suggest that the density profile is actually shallower than NFW towards the centre with an Einasto profile giving a better fit (Springel et al. 2008). However, since we are not interested in the central regions, the NFW profile is an appropriate choice.

it takes for this shock to cross the diameter of the satellite:

$$t_{\text{rps}} \sim 2 \int_0^{r_v} \frac{dr}{v_{\text{sh}}(r)}. \quad (5)$$

The average mass removal rate from RPS is then given by:

$$\dot{m}_{\text{rps}} \sim \frac{m_{\text{sat}}(< r_{\text{rps}}) - m_{\text{sat}}(< r_{v,\text{sat}})}{t_{\text{rps}}}. \quad (6)$$

2.1.2 Tidal Stripping (TS)

Tides remove gas and dark matter from the satellite as it falls into the host. The tidal radius r_t , defined as the radius where the external differential tidal force from the host exceeds the binding force of the satellite, is approximately given by (e.g. Taylor & Babul 2001):

$$r_t^3 = \frac{Gm_{\text{tot}}(< r_t)}{w^2 + G[2M(< r)/r^3 - 4\pi\rho_{\text{host}}(r)]}, \quad (7)$$

where w is the angular speed of the satellite located at a distance r from the host, which has a mass and density profile $M(< r)$ and $\rho_{\text{host}}(r)$ respectively. The material outside r_t is tidally removed from the system within a time scale $t_{\text{ts}} = t_{\text{orb}}/A$ where $t_{\text{orb}} = 2\pi/w$ is the instantaneous orbital time and A is an efficiency parameter. It is important to note that Eq. (7) is only a rough approximation². The uncertainties associated with this equation are parameterised by the factor A that has values between 1 and 6 according to numerical simulations of dark matter subhaloes orbiting host haloes (Taylor & Babul 2001; Zentner et al. 2005; Diemand et al. 2007). We take a fiducial value of $A = 3.5$ as found by Gan et al. (2010), and define the mass removal rate due to TS as:

$$\dot{m}_{\text{ts}} = \frac{m_{\text{sat}}(< r_t) - m_{\text{sat}}(< r_{v,\text{sat}})}{t_{\text{ts}}}. \quad (8)$$

Besides RPS and TS, the corona of the satellite can be subjected to other mass loss mechanisms which we mention subsequently (closely following Nulsen 1982).

2.1.3 Laminar viscous stripping

If viscosity is relevant in the ICM, then there will be a drag in the corona of the satellite resulting in a gas mass loss which is roughly given by (ignoring gravity):

$$\dot{m}_{\text{visc}} \approx \left(\frac{12}{\text{Re}}\right) \pi r_{\text{sat}}^2 \rho_{\text{host}} v_{\text{sat}}, \quad (9)$$

where r_{sat} is the instantaneous maximum radial extent of the corona of the satellite and Re is the Reynolds number:

$$\text{Re} = 2.8 \left(\frac{r_{\text{sat}}}{\lambda_{\text{host}}}\right) \left(\frac{v_{\text{sat}}}{c_{s,\text{host}}}\right), \quad (10)$$

with λ_{host} being the effective mean free path of ions in the ICM. In the absence of magnetic fields and for Coulomb collisions this is given by (Spitzer 1956):

$$\lambda_{\text{host}} \approx 11 \text{ kpc} \left(\frac{T_{\text{host}}}{10^8 \text{ K}}\right)^2 \left(\frac{\rho_{\text{host}}/m_H}{10^{-3} \text{ cm}^{-3}}\right)^{-1}. \quad (11)$$

For Eq. (9) to be applicable, the gas flow needs to be

² For instance, the tidal radius is only well-defined for circular orbits, whereas realistic orbits are in general eccentric.

laminar around the boundary of the satellite, i.e., $\text{Re} \leq 30$, and also $\lambda_{\text{host}} \leq r_{\text{sat}}$. Since $T_{\text{host}}^2/\rho_{\text{host}} \propto r^{1.9}$ for the NFW profile (and for the temperature given by the EoS assuming hydrostatic equilibrium), $\lambda_{\text{host}}(r) \leq \lambda_{\text{host}}(r_{v,\text{sat}})$. At the virial radius of the host, the mean free path is of $\mathcal{O}(1 \text{ kpc})$ and since $v_{\text{sat}}/c_{s,\text{host}} \gtrsim 1$ (the initial shock is transonic), the Reynolds number is then very large and viscosity is irrelevant (see Table 2). Due to RPS and TS, r_{sat} will be reduced as the satellite spirals inwards to the centre of the host but the ratio $r_{\text{sat}}/\lambda_{\text{host}}$ will certainly remain very large. The changes in the ratio $v_{\text{sat}}/c_{s,\text{host}}$ will depend strongly on the orbit but will likely remain larger than 1, increasing towards pericentre, and dropping below 1 near apocentre. If apocentre is near the virial radius of the group (cluster) and the radius of the satellite has been reduced by a significant factor, then Re could drop below 30 in the cluster environment. This is unlikely to happen in the group environment because the mean free path of the ions in the ICM is an order of magnitude smaller than in the cluster environment. We neglect viscous stripping in the remainder of this work.

2.1.4 Evaporation due to thermal conduction

The rate of evaporated mass due to thermal conduction from a spherical cloud embedded in a hot tenuous gas, neglecting gravity, radiation, ionization and magnetic fields, is approximately given by (Cowie & McKee 1977):

$$\dot{m}_{\text{evap}} \approx 4\pi r_{\text{sat}}^2 \rho_{\text{host}} c_{s,\text{host}} \phi_s F(\sigma_0), \quad (12)$$

where ϕ_s is a parameter of $\mathcal{O}(1)$ and $\sigma_0 \equiv 1.84\lambda_{\text{host}}/r_{\text{sat}}\phi_s$ determines when the regime of classical conductivity still applies. This happens when the mean free path is short compared to the temperature scale height $L_T = T/|\nabla T|$ between the boundary of the cloud and the hot gas surrounding it ($\lambda_{\text{host}} \ll L_T$); in this regime, $F(\sigma_0) = 2\sigma_0$. For the set of interacting systems we are considering, $r_{\text{sat}}/\lambda_{\text{host}} > \mathcal{O}(100)$, thus, $\sigma_0 < \mathcal{O}(0.01)$, which makes the mass loss rate due to thermal conduction much lower than that of the other processes for the group environment (see Table 2). For the cluster environment, evaporation is still subdominant but it cannot be entirely neglected.

2.1.5 Turbulent Stripping (Kelvin-Helmholtz Instability)

If the inertial forces in the surface layers between the two gases are larger than those related to viscosity (i.e. if $\text{Re} > 30$), then the velocity shear between the layers will drive KH instabilities. The collision between the coronae of the satellite and the ICM also drives a reverse shock that propagates into the ICM (contrary to the forward shock propagating into the satellite and related to RPS). Since, typically, $v_{\text{sat}} \sim c_{s,\text{host}}$ at infall, this shock is generally weak. The post-shock flow in the vicinity of the boundary of the satellite, where the instabilities develop, will then be subsonic (propagating at a speed v_{ps} , see Eq. A2). Under this assumption, and taking into account the compressibility of the gas flow, the mass loss rate for complete stripping due to KH instabilities is:

$$\dot{m}_{\text{KH}} \sim \pi r_{\text{sat}}^2 \rho_{\text{host}} v_{\text{ps}}. \quad (13)$$

In this equation, the dominant wavelength of the perturbations is of the order of the radius of the corona of the

Table 2. Typical values for the parameters defining different processes of gas removal for a MW-size galaxy falling into a group/cluster (see Table 1). Times are given in Gyr and mass loss rates in M_\odot/yr .

Environment	r_{rps}/r_v	t_{rps}	\dot{m}_{rps}	r_t/r_v	t_{ts}	\dot{m}_{ts}	$\lambda_{\text{host}}/r_v$	Re	t_{KH}	\dot{m}_{KH}	\dot{m}_{evap}
galaxy-group	0.78	2.1	15	0.65	2.4	22	7×10^{-4}	4800	1.2	39	0.5
galaxy-cluster	0.45	1.9	50	0.65	2.4	22	1.4×10^{-2}	250	0.56	53	23

satellite. This is because the stripping process begins with perturbations that have shorter wavelengths; as they develop, they smooth the velocity gradient between the layers making the interface thicker. This damps modes with wavelengths smaller than the thickness of the interface, while larger wavelength modes continue growing, stripping more material and making the interface thicker. This process continues until the layer has a thickness of order r_{sat} .

As we mentioned before, the velocity flow near the layer is expected to be subsonic. We estimate the values of v_{ps} by solving a one dimensional shock tube problem (see Appendix A) using the value of the hydrodynamical variables at the beginning of the interaction (assuming initial pressure equilibrium between both systems). We find $v_{\text{ps}} \sim 208$ (260) km/s for the group (cluster) environments resulting in mass loss rates which are of the order of those by RPS and TS (see Table 2). The time scale for the formation of the largest wavelength instabilities can be roughly estimated for an ideal case where the fluids are incompressible, the surfaces are flat, gravity is neglected, and the overdensity near the boundary is in the linear regime: $\delta = \rho_{\text{sat}}/\rho_{\text{host}} - 1 \ll 1$. In this case (e.g., Drazin & Reid 1981):

$$t_{\text{KH}} \sim \frac{2r_{\text{sat}}}{v_{\text{sat}}}, \quad (14)$$

which is of the order of the sound crossing time.

Gravity and density stratification of the gas are stabilizing effects acting against the development of KH instabilities. By assuming that the interface has a sharp density discontinuity between the gas in the satellite ρ_2 and the ICM gas ρ_1 , Murray et al. (1993) found that the dominant wavelength for gas ablation, $k = 2\pi/r_{\text{sat}}$, is stable if:

$$g > \frac{2\pi\rho_1\rho_2v_{\text{sat}}^2}{r_{\text{sat}}(\rho_2^2 - \rho_1^2)}, \quad (15)$$

where $g = Gm_{\text{tot}}(< r_{\text{sat}})/r_{\text{sat}}^2$ is the gravitational acceleration at the interface. This condition can be rewritten in terms of the gravitational restoring pressure (Eq. 4):

$$P_{\text{restore}}(r_{\text{sat}}) > \frac{2\pi\alpha_g\rho_1v_{\text{sat}}^2}{1 - (\rho_1/\rho_2)^2}. \quad (16)$$

The rhs of Eq. (16) is expected to be much larger than the restoring force in the outskirts of the satellite, and thus, the corona will not be stabilized by its own self-gravity but the mass loss rate in Eq. (13) is probably going to be reduced. Other physical processes, such as magnetic fields (e.g. Malagoli et al. 1996) and radiative cooling (e.g. Vietri et al. 1997), might stabilize the corona of the satellite.

Given the parameters of the interacting galaxies, it seems likely that RPS, TS and KH instabilities will act on similar time scales, competing to remove the gas from the corona of the satellite. Besides gas removal, all these processes will also mix the stripped gas with the gas in the ICM with important consequences as we discuss below.

2.2 Cooling due to mixing

As the satellite orbits the host, it loses energy and angular momentum due to dynamical friction (Chandrasekhar 1943) eventually merging completely with the host. The typical time scale for this to happen is $\sim 4(23)$ Gyr for the satellite merging into the group (cluster) (following the study of Boylan-Kolchin et al. 2008). This implies that the satellite will remain in orbit for a reasonable time before getting too strongly disrupted. Thus, the gas removed from the satellite will have enough time to mix with the ICM, changing its properties. In the following, we consider this gas mixing process, inspired by the study of Marinacci et al. (2010).

The coronal gas is being removed at a rate given by the different stripping processes. If we take the mass loss rate by RPS as a reference, then $\dot{m}_{\text{rem}} = \alpha_{\text{rem}}\dot{m}_{\text{rps}}$, with $\alpha_{\text{rem}} \gtrsim O(1)$ representing the mass loss for other processes. The removed gas mixes with the ICM (possibly quite efficiently due to the turbulent flow generated by KH instabilities) and falls behind the satellite forming a wake. In the time it takes the satellite to move a distance s , the gas mixture occupies a volume $V_w = A_w s$, where A_w is the cross section of the wake. If we neglect the compressibility of the gas, then the mass from the corona and the ICM contained within V_w is: $M_w = M_{\text{host,w}} + M_{\text{sat,w}} = A_w s \rho_{\text{host}} + \dot{m}_{\text{rem}} s / v_{\text{sat}}$. If the gases in the corona and the ICM have the same composition, then the temperature of the mixture is just:

$$T_m = \frac{M_{\text{host,w}}T_{\text{host}} + M_{\text{sat,w}}T_{\text{sat}}}{M_{\text{host,w}} + M_{\text{sat,w}}} = \frac{A_w\rho_{\text{host}}T_{\text{host}} + \dot{m}_{\text{rem}}T_{\text{sat}}/v_{\text{sat}}}{A_w\rho_{\text{host}} + \dot{m}_{\text{rem}}/v_{\text{sat}}}. \quad (17)$$

Note that thermal conduction is necessary to reach this temperature, but this can happen efficiently on small scales due to turbulent mixing. Depending on the relative difference between the gas from the satellite being deposited in the wake $\dot{m}_{\text{rem}}/v_{\text{sat}}$ to that of the ICM $A_w\rho_{\text{host}}$, the temperature of the mixture can decrease significantly relative to T_{host} , down to a minimum of T_{sat} .

The characteristic scale for the cross section of the wake is given by a combination of the gravity of the satellite, the inertia of the stripped gas and turbulent effects. For simplicity, we parametrize it as $A_w = \beta\pi r_s^2$, where r_s is the scale radius of the halo of the satellite: $r_s = r_{v,\text{sat}}/c$ (with c being the concentration of the halo), and β is a free parameter which in the absence of turbulence is mainly set by the velocity of the satellite³. We note that in reality, the

³ This cross section seems to be a good guess according to the results we found for a low resolution simulation analogous to the non-radiative simulation described in Section 3 for a subsonic collision ($v_{\text{sat}} = 150$ km/s). We found that the cross-sectional radius of the wake separating the gas in the ICM that flows without

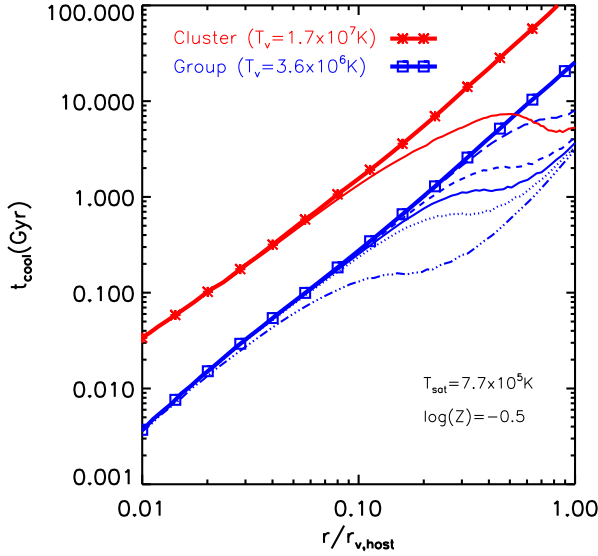


Figure 1. Cooling time as a function of radius for a group/cluster with an NFW density profile under hydrostatic equilibrium. The thick solid lines are for an isolated system; the thin solid lines show what would happen if gas in the ICM at different radii mixed with coronal gas removed from an infalling satellite ($T_{\text{sat}} = 7.7 \times 10^5 \text{ K}$) moving with a constant speed equal to the virial velocity of the group/cluster (the cooling time refers in this case to the gas in the mixture). The gas is removed at a constant rate $\dot{m}_{\text{rem}} = \alpha_{\text{rem}} \dot{m}_{\text{rps}}$ and mixes with the ICM in a region with a cross sectional area $A_w = \beta \pi r_s^2$. The thin solid lines are for $\alpha_{\text{rem}} = \beta = 1$. The dashed (dotted) lines are for $\alpha_{\text{rem}} = 1/2$ (2) and the long-dashed (dotted-dashed) lines are for $\beta = 10$ (1/10).

gas mixes across layers of different sizes in the turbulent flow creating a broad distribution of A_w values.

The time scale for gas to lose its thermal energy due to radiative losses is given by:

$$t_{\text{cool}} = \frac{3/2 n k_B T}{n_e n_H \Lambda_{\text{cool}}(T, Z)}, \quad (18)$$

where $n = \rho_{\text{host}}/(\mu m_H)$, n_e and n_H are the number densities for electrons ($n_e = 0.52n$) and hydrogen, respectively; and $\Lambda_{\text{cool}}(T, Z)$ is the cooling function that depends on temperature and metallicity. We obtain the cooling function from the tables given by Gnat & Sternberg (2007).

Fig. (1) shows the cooling time for the gas mixture as a function of the distance to the centre of the group (cluster) assuming that the ICM in the host mixes with gas from the satellite with a single temperature ($T_{\text{sat}} = T_{v,\text{sat}}$). We also assume that the density of the mixture is the same as the density of the host⁴, and that the mass loss rate and velocity of the satellite remain constant with radii. We have used a metallicity of $\log_{10}(Z/Z_{\odot}) = -0.5$, which is representative of the values found in groups and clusters

mixing with the one that mixes is $\sim r_s$, i.e., $\beta = 1$. For higher velocities, β is likely to increase asymptotically to $(r_v/r_s)^2$.

⁴ Note that it is perhaps more reasonable to assume that the mixture will have the same pressure as the ambient ICM; in this case, its density will be higher and thus its cooling time will be lower than the one we have estimated.

(Rasmussen & Ponman 2009). The thick solid lines show the reference cases where there is no mixing, in blue and red for the group and cluster, respectively. The thin blue and red lines show the case when mixing is effective, with $\alpha_{\text{rem}} = \beta = 1$ for the group and cluster, respectively. Only for the group, we show lines where the ratio $\dot{m}_{\text{rem}}/v_{\text{sat}}$ is decreased (increased) by a factor of 2, dashed (dotted) blue, and for changes in the parameter β increasing (decreasing) it by a factor of 10, long-dashed (dotted-dashed) blue. The former of these explores variations in the efficiency of gas removal, and the latter on the effective size of the region where material mixes.

The regions where the different assumptions made to arrive at Fig. (1) are likely to be true, are those close to the outskirts of the host. We see that for $r/r_{v,\text{host}} \sim 0.6$ the cooling time of the mixed material is of $\mathcal{O}(1 \text{ Gyr})$ for the group environment, which is an order of magnitude lower than the cooling time of the ambient ICM. For the cluster environment, the reduction in the cooling time is also quite substantial but certainly above a few Gyrs.

If a volume element of gas can cool down quickly enough by radiating its thermal energy, then, in the absence of any source of heating, it will lose all its pressure support and collapse in a free-fall time:

$$t_{\text{ff}} = \sqrt{\frac{3\pi}{32G\rho_{\text{local}}}}. \quad (19)$$

The condition $t_{\text{cool}} = t_{\text{ff}}$ separates the gas clouds that can cool down effectively from those that cannot. The local free-fall time for gas at $r \sim 0.6r_{v,\text{host}}$ in the group(cluster) environment is $\sim 4 \text{ Gyr}$.

Therefore, from the theoretical expectations described in this section we conclude that: *the coronal gas removed from the infalling satellite will mix with the ICM of the host, creating a mixture with a cooling time potentially lower than the local free-fall time. The net effect is an increase in the cooling efficiency of the gas mixture trailing behind the merging satellite, relative to the ambient ICM.* Of course, the gas mixture will have a cooling time which is larger than that of the initial corona.

Note that we have chosen a mass for the MW-size galaxy which is at the low end of the range of Milky-Way halo masses allowed by current estimates (see e.g. section 5.1 of Boylan-Kolchin et al. 2012), which results in a virial temperature for the corona that is relatively low compared to other estimates (e.g. Fukugita & Peebles 2006 estimate $T_v = 1.4 \times 10^6 \text{ K}$ since they assume $M_v = 2.6 \times 10^{12} M_{\odot}$). A hotter corona would result in a reduction of the cooling efficiency of the mixed ICM gas. We have also chosen a low-mass group ($10^{13} M_{\odot}$), corresponding to a galaxy-group merger mass ratio of 1/10. Mergers with lower mass ratios are typically more common in a cosmological setting (see e.g. Fakhouri et al. 2010), and as implied by Fig. (1) for the case of the galaxy-cluster collision, a merger with a group of higher mass (virial temperature) would increase the temperature of the gas mixture. Nevertheless, the 1/10 galaxy-group merger we are taking as a reference should be common enough to be of interest. We leave the analysis in a full cosmological setting for a future work and concentrate in the rest of this paper on the formation and properties of the wakes produced by the galaxy-group interaction.

In the previous analysis, we neglected the compression

of the gas during mixing, which could in principle reduce the cooling time and the free fall time even further. However, since an adiabatic compression would also increase the temperature of the gas (heating the mixture instead of cooling it), it might be that the two effects cancel each other. We answer this question in the following section.

It is in principle possible that a fraction of the gas trailing behind the satellite is gravitationally re-accreted. However, we find that for the parameters in Table 1, the presence of the satellite in the environment of the group(cluster) results in a Bondi radius $\lesssim 53(11)\text{kpc}$, which is smaller than the virial radius of the satellite. Since RPS happens fairly rapidly, the effective radius of the corona is quickly reduced while the mass of the dark matter satellite remains fairly the same at first since TS is expected to act more slowly (see Table 2). Nevertheless, the stripping of the gas is not enough to reduce r_{sat} to the Bondi radius. For this to happen in the group (cluster) medium, the stripping efficiency would need to be much higher, followed by a period of relatively low orbital velocities (low compared to the virial velocity of the host). The satellite could then potentially accrete material from the ICM. Although this situation is not common for the systems we are studying, in the case of the galaxy-group collision, a “fine-tuned” orbit could potentially have a Bondi radius smaller than the extent of the corona of the satellite near apocentre.

3 SIMULATIONS

We use the Eulerian code FLASH (Fryxell et al. 2000), that uses an AMR technique to solve the hydrodynamical equations for the fluid. With this technique, FLASH is able to increase the resolution of the grid solver in the regions of most interest while keeping a coarser grid elsewhere. FLASH also includes the possibility of adding particles to the simulation in two varieties: *active* and *passive*. The former have mass and participate in the dynamics of the system, and we use them to simulate the dark matter halo. Passive particles have no mass and do not contribute to the dynamics, they are Lagrangian tracers of the flow and are useful to study the degree of mixing. The code uses a particle-mesh method to map the quantities from the mesh into the particles and vice versa. The Euler equations are solved using a piecewise-parabolic method (Colella & Woodward 1984) and the gravitational potential is solved using a parallel multigrid solver (Ricker 2008).

3.1 Initial conditions and setup

The satellite consists of a spherical distribution of collisionless dark matter and gas with an ideal equation of state. Both of these fluids have a density profile given by Eq. (1). Dark matter is simulated with a set of N particles with their positions and velocities given by an algorithm based on the method presented in Kazantzidis et al. (2004). To assign the position of each particle, we randomly draw a value of the enclosed mass $M(< r)$ in the interval $[0, M_v]$ and then invert the function $M(< r)$ to find the distance of that particle to the centre of the halo. The velocities of the dark matter particles are assigned from their actual energy

distribution function given by the Eddington formula (e.g. Binney & Tremaine 1987):

$$f(\varepsilon) = \frac{1}{\sqrt{8\pi^2}} \left[\int_0^\varepsilon \frac{d^2\rho}{d\Psi^2} \frac{d\Psi}{\sqrt{\varepsilon - \Psi}} + \frac{1}{\sqrt{\varepsilon}} \left(\frac{d\rho}{d\Psi} \right)_{\Psi=0} \right], \quad (20)$$

where $\Psi = -\phi$ is the relative gravitational potential and ε is the relative energy $\varepsilon = \Psi - v^2/2$. We construct a table with values of ε and $f(\varepsilon)$ that allows us to linearly interpolate for any value of the relative energy. The magnitude of the velocity of each particle is then drawn at random from the distribution function $2[\Psi(r) - \varepsilon]^{1/2} f(\varepsilon)$ using a rejection sampling method (von Neumann 1951). The direction of the position and velocity vectors is chosen at random from the unit sphere. This method ensures that the dark matter halo is a system in equilibrium (except of course from imbalances caused by discreteness effects).

Gas is simulated by a hierarchy of cells using the AMR technique. The initial pressure in the cells is given by the condition of hydrostatic equilibrium as described at the beginning of Section 2. The velocities of the particles are set to zero. Finally the gas is set to have a mean molecular weight of $\mu^{-1} = 1.71$.

In this way we generate an initial equilibrium configuration for a MW-size galaxy having the parameters given in Table 1. We have tested that this system remains in equilibrium for at least $\sim 5\text{Gyr}$ when evolved in isolation. Nonetheless, two clear features appear in the density profile during this time: a small core ($\sim 5\text{kpc}$) that develops in the centre due to the limited resolution of the grid, and a small fraction of the dark matter particles ($\sim 2\%$) expand to larger radii due to the tapering of the density profile at the virial radius.

Finally, to simulate the ICM, the system is surrounded by gas with constant density (10^{-28}g cm^{-3}) and temperature ($3.6 \times 10^6\text{K}$) moving relative to the satellite with a speed $v_{\text{sat}} = V_{\text{v,group}} = 315\text{ km/s}$. The simulation box has a length of 1.9 Mpc with periodic boundary conditions⁵. The resolution of the simulation uses 32 cells for the coarsest level with 6 levels of refinement to give a maximum spatial resolution of $\sim 1\text{ kpc}$. We use 50^3 active particles to represent the dark matter halo of the MW-size galaxy, and 100^3 (50^3) tracer particles to sample the initial gas density distribution of the ICM (satellite).

We consider two simulations, one without radiative losses and one where the gas is allowed to cool radiatively. This allow us to understand the impact of cooling in the formation of the turbulent wake: efficient cooling in the corona of the satellite prior to the removal of the gas would increase its density and reduce its sound speed, and hence suppress the KH instabilities, greatly reducing the amount of stripped gas. Central feedback is expected to reduce the cooling rate in the satellite, preventing a catastrophic collapse that would otherwise occur both in nature and in the simulations (this collapse also leads to prohibitive simulation time steps). To mimic the effects of feedback we multiply the cooling rate by a function of the distance to the center of the satellite: $1 - 1/(1 + (r/r_c)^3)$ where $r_c = 0.15 r_v$. In addition, we introduce a temperature floor of 10^5K , below which the gas

⁵ Periodic boundary conditions are necessary to use the parallel multigrid solver for the Poisson equation in the version of FLASH we used.

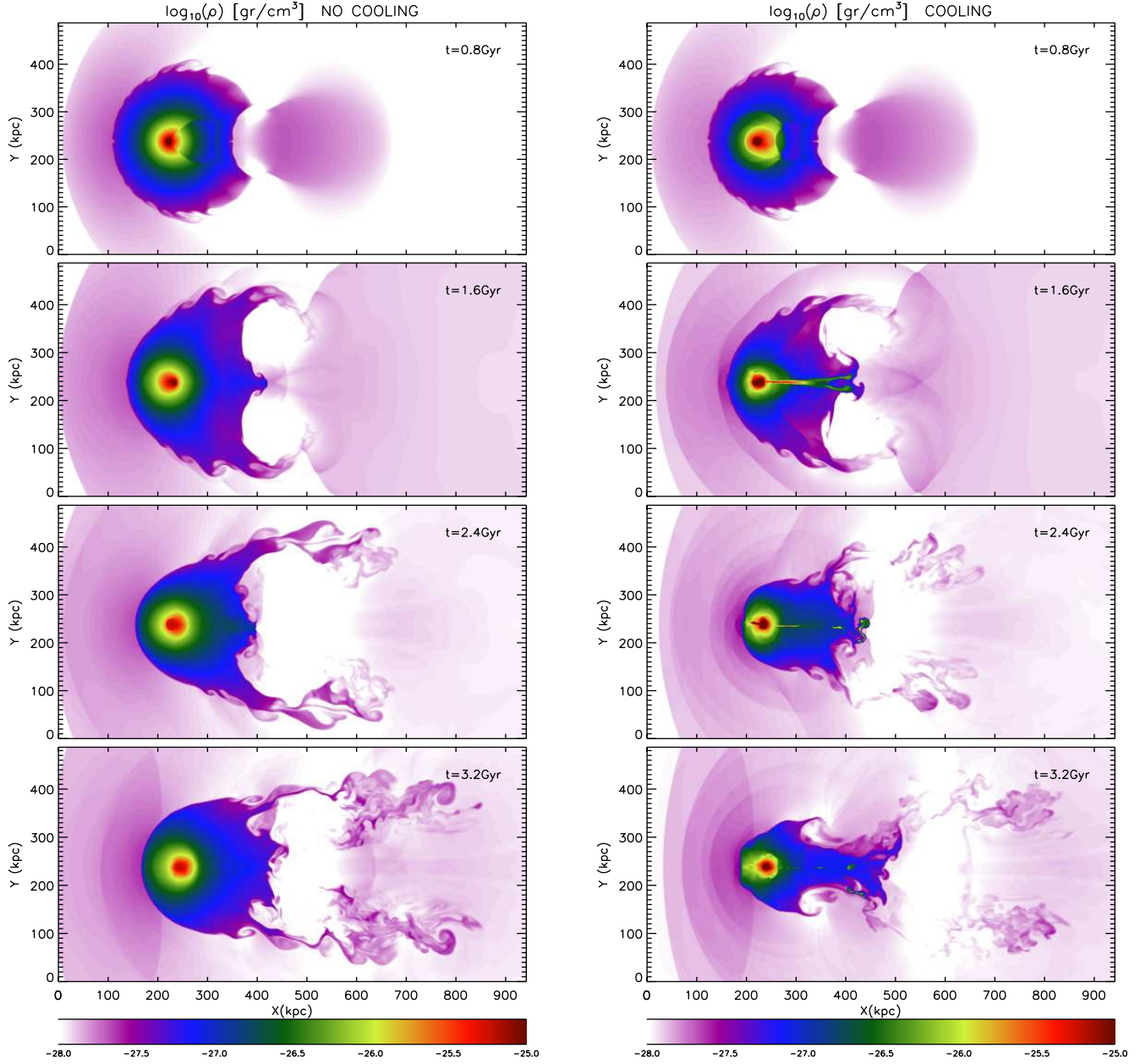


Figure 2. Slices of gas density (logarithmic) in the XY plane through the middle of the simulation box for the non-radiative (left) and dissipative (right) simulations at $t = 0.8, 1.6, 2.4$ and 3.2 Gyr.

does not cool further. We remark that this feedback does not affect the regions of interest, namely outside $\sim 0.7r_v$ (the stripping radius) and that we do not intend to give a realistic feedback model but simply to attenuate the central overcooling. We simulate a single gas species with a metallicity of $\log_{10}(Z/Z_{\odot}) = -1.5$ in both, the satellite and the ICM. Although in a realistic setting the gas is likely to have different metallicities according to its position relative to the center of the satellite, and to the center of the low-mass group, we choose this value for simplicity and because it further help us reducing the central collapse of the corona. We note that this value is roughly of the order of what is found in simulations of MW-size haloes near the virial radius (see Fig. 9 of van de Voort & Schaye 2012).

4 RESULTS

Fig. (2) shows slices of the XY plane through the middle of the simulation box for the density of the gas for the non-radiative (left panels) and dissipative (right panels) cases at four output times $t = 0.8, 1.6, 2.4$ and 3.2 Gyr from top to bottom, respectively. The effect of RPS and the development of KH instabilities are clearly seen. In the top panels, we see how the shock has propagated through the satellite and is passing through its dense centre, whereas in the outskirts, it has traversed most of the satellite. By $t \sim 2.4$ Gyr, the shock has crossed the satellite completely and the gas removed by RPS is already forming clear trailing wakes. This roughly

agrees with our estimate of the RPS time scale to be of the order of 1.8 Gyr (see Table 2 and Appendix A).

In the dissipative simulation, the central collapse is already apparent after $t \sim 1$ Gyr with the formation of a dense and cold core. Although the artificial suppression of cooling prevents the central collapse from continuing further, the contraction of the corona is large enough to significantly reduce the amount of stripped gas. However, the presence of the trailing wakes and the effect of turbulence are still evident. The linear, dense and cold feature to the right of the center of the satellite is caused by the asymmetry of the problem and the inclusion of a spherically symmetric cooling suppression. Although the shape of the central “inner” wake is affected by this feature, there is only a minor impact on the extended “external” wakes that participate in most of the mixing with the ICM.

4.1 Turbulence and gas mixing

After $t \sim 1$ Gyr, the stripped gas starts mixing efficiently with the ICM through the turbulence generated by KH instabilities. From an initial look at the density and temperature of the gas at $t = 3.2$ Gyr, it seems that the gas mixture has twice the density and nearly half the temperature of the ambient ICM. To give a first estimate of the amount of mass that makes the bulk of the mixed phase, we show in Fig. (3) a mass-weighted temperature histogram of all the mass contained within a box that extends above and below the slice shown in Fig. (2) with a thickness of ~ 490 kpc. In this way, the volume covered by this box encloses all the mass that is being mixed, the satellite, and of course a fraction of the ICM that is not involved in the mixing. The black histogram is for $t = 0$ Gyr, while the blue and red are for $t = 3.2$ Gyr for the simulations with and without cooling, respectively. The initial gas distribution within the satellite is clearly seen around 10^6 K as a “cold” phase, as well as the singled-value “hot” phase in the ICM to the right. At the end of the non-radiative simulation, the gas in the satellite has been shock-heated while the ICM has been adiabatically compressed and expanded (see below). For the dissipative simulation, the centre of the satellite has partially collapsed, forming a cold core with a temperature given by the imposed floor of 10^5 K. The rest of the gas however seems to be distributed in a similar way in both simulations; in particular, the formation of a “warm” phase at $T \sim 2 \times 10^6$ K is apparent in the figure for both cases. We show below that this phase is actually formed by the mixture of the two phases and not just by the gas stripped from the satellite.

The upper panels of Fig. (4) give an idea of the degree of mixing between the fluids at the end of the non-radiative (left panel) and dissipative (right panel) simulations. They show the distribution of tracer particles that were set at $t = 0$ to sample the density distribution in the satellite (red) and in the ICM (black). In the figures, a projection of this distribution at $t = 3.2$ Gyr is shown for a slab with a thickness of 50kpc^6 . The objective of this figure is to show that the two fluids originally separated are thoroughly mixed by

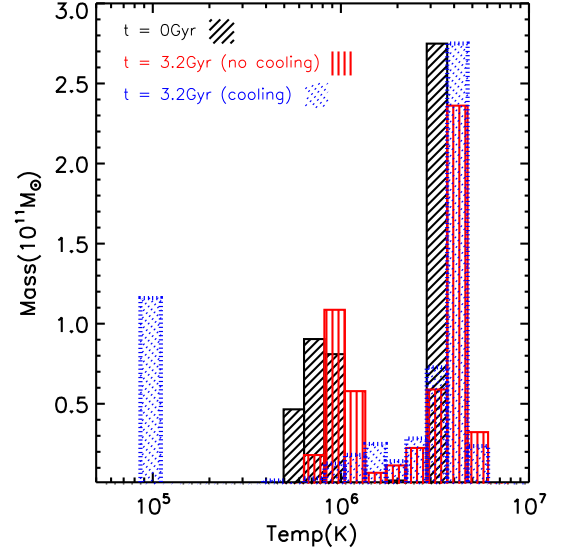


Figure 3. Mass-weighted histogram of the temperature within a reduced volume of the simulation box, see text for details. The black histogram is for the initial simulation time, whereas the red and blue histograms are for the final simulation time for the cases without and with radiative cooling, respectively.

the turbulent motions in the plumes. The degree of mixing is similar in both simulations.

The bottom panels of Fig. (4) are a slice through the middle of the simulation box showing the cooling time, constructed using the temperature and density of the gas at $t = 3.2$ Gyr and assuming a single metallicity, $\log_{10}(Z/Z_{\odot}) = -0.5$, representative of the intragroup gas. In reality, the cooling time of the gas mixture would depend on the mass-weighted metallicities of the species being mixed. Since these are uncertain, and for simplicity, we have chosen a constant metallicity, but of course, the absolute value of the cooling times reported in this work are metallicity-dependent. We see that in the trailing wakes where the gas mixes more efficiently, the cooling times have decreased by up to an order of magnitude compared to the original cooling time in the ICM.

Fig. (5) shows the position of the tracer particles (in red and black for the satellite and ICM, respectively), within the slab shown in the upper panel of Fig. (4) (i.e., within a box of volume $942 \times 487 \times 50$ kpc³) in a temperature-density diagram at different simulation times: $t = 0.1, 0.8, 2.4$ and 3.2 Gyr clockwise starting from the upper left of each set of panels. The set to the left (right) corresponds to the simulation without (with) radiative cooling. The dotted lines are lines of constant cooling time from 100 Gyr to 0.1 Gyr going from left to right. The thick black solid line shows the locus of points where the cooling time equals the local free-fall time ($t_{\text{ff}} = t_{\text{cool}}$). Finally, the dashed line is a reference marking processes that conserve entropy (defined here as $S \propto T/\rho^{2/3}$).

Since the number of tracer particles in the satellite is high (particularly in the center of the satellite), we have randomly selected a smaller sample to plot in Fig. (5), except in the region around the wakes for the last two time

⁶ The tracer particles sample the gas distribution with lower resolution than the mesh cells, particularly for the ICM where the initial inter-particle separation is ~ 15 kpc.

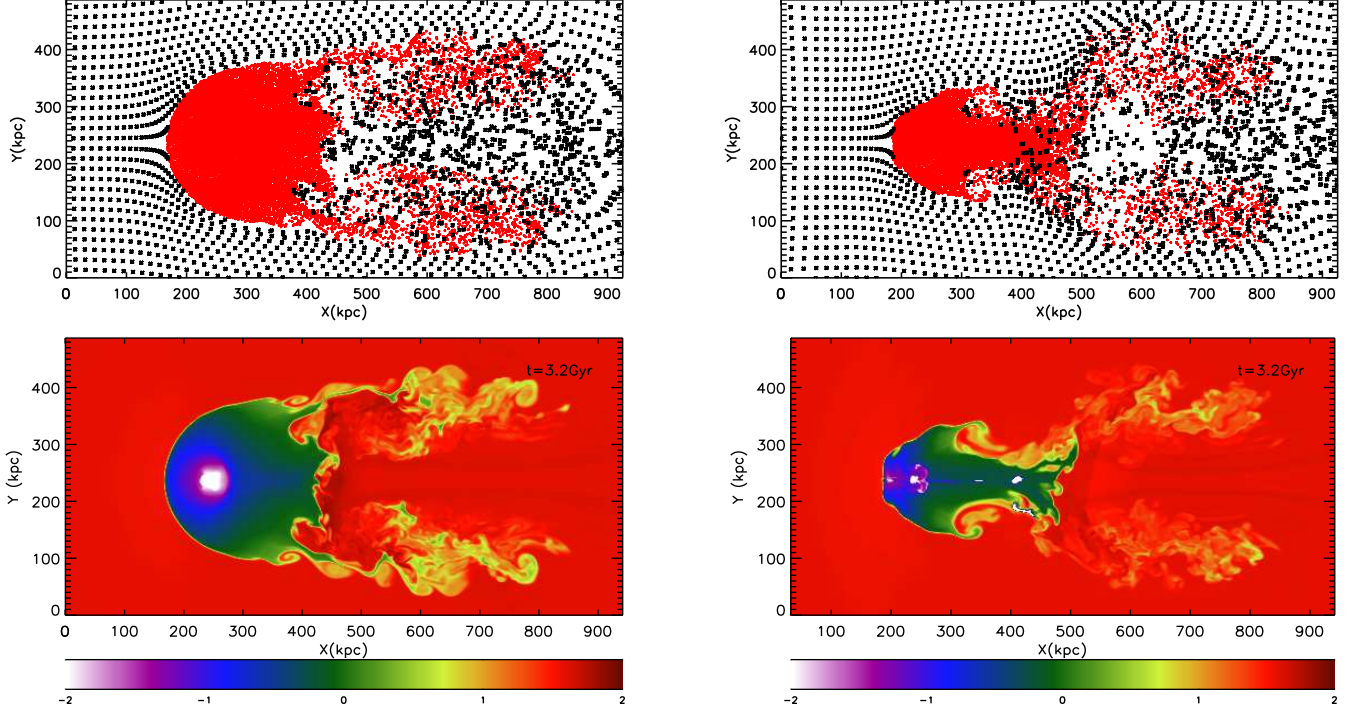


Figure 4. *Upper panels:* Distribution of tracer particles after $t = 3.2$ Gyr for a slab through the middle of the simulation box with a thickness of 50 kpc; red and black for the satellite and ICM, respectively. *Bottom panels:* Slice in the XY plane through the middle of the simulation box at $t = 3.2$ Gyr showing the values of the cooling time (logarithmic) assuming $\log_{10}(Z/Z_{\odot}) = -0.5$. The panels on the left (right) correspond to the simulation without (with) radiative cooling.

outputs, bottom panels, where the tracers are shown with bigger symbols. We have verified that this random subsample traces the distribution of the full sample and remark that this was done simply for plotting purposes. This region around the wakes is the one corresponding to $X > 500$ kpc in Fig. (2) (see section 4.2).

Initially, the ICM gas represents a single point in this diagram ($\rho = 10^{-28} \text{ g cm}^{-3}$, $T = 3.6 \times 10^6 \text{ K}$) and the gas in the satellite is distributed according to the equilibrium configuration. In the first 100 Myr, the gas in the ICM immediately surrounding the satellite compresses upstream and expands downstream, conserving its entropy. The gas on the satellite is compressed and shocked upstream; the gas loosely bound to the satellite begins to be removed. As the shock traverses the satellite, it heats and compresses the gas within it, removing material from the outskirts while gravity tends to restore the original gas distribution; the distribution within the inner regions will remain distorted though, since the shock causes an irreversible change in the gas.

In the dissipative simulation, the gas that remains within the satellite is additionally subjected to the central collapse, which is suppressed in the innermost regions by the feedback-like mechanism we have introduced. This creates a gas distribution that is highly dispersed in the phase diagram (the coldest and densest material is not explicitly shown in Fig. 5 since we concentrate on the regions where mixing happens). On the other hand, the behaviour of the gas in the outskirts of the satellite, and outside in the ICM, is qualitatively similar to the one in the non-radiative simulation. In particular, most of the ICM evolves along a path of

constant entropy (expanding and contracting driven by the relative motions of the fluids, and the pressure support and gravity of the satellite). At $t \sim 1$ Gyr, a fraction of the ICM is clearly mixing with the stripped gas increasing its density and decreasing its temperature. By $t = 3.2$ Gyr, a mixed phase of gas is apparent in the figure with $T \sim 2 \times 10^6 \text{ K}$ and $\rho \sim 2 \times 10^{-28} \text{ g cm}^{-3}$. This confirms the initial visual impression given by the bottom panels of Fig. (2), and also proves that the “warm” phase shown in Fig. (3) is a mixed phase formed by gas from the satellite and the ICM.

By looking at the lines of constant cooling time, we see that the mixed phase reaches values of $t_{\text{cool}} \sim 5$ Gyr, considerably lower than the initial cooling time of ~ 40 Gyr. We also see that by the end of the simulation, the mixed phase is approaching the locus of points $t_{\text{ff}} = t_{\text{cool}}$ that separates the gas that can cool efficiently from the one that cannot.

4.2 Properties of the wakes

We define the wakes as the trailing structures that are clearly distinguished in Fig. (2) at $X > 500$ kpc. By doing so, we exclude the material that is not bound to the satellite but is still attached to it. This gas will be stripped in the future and added to the trailing wakes, but since this gas is clearly not participating in the mixing we omit it from the analysis. We note that although this definition is arbitrary, the properties of the wakes at a given time serve as an approximate reference for the properties at other times. With such definition, we find that at $t = 3.2$ Gyr roughly 50%, 55% of

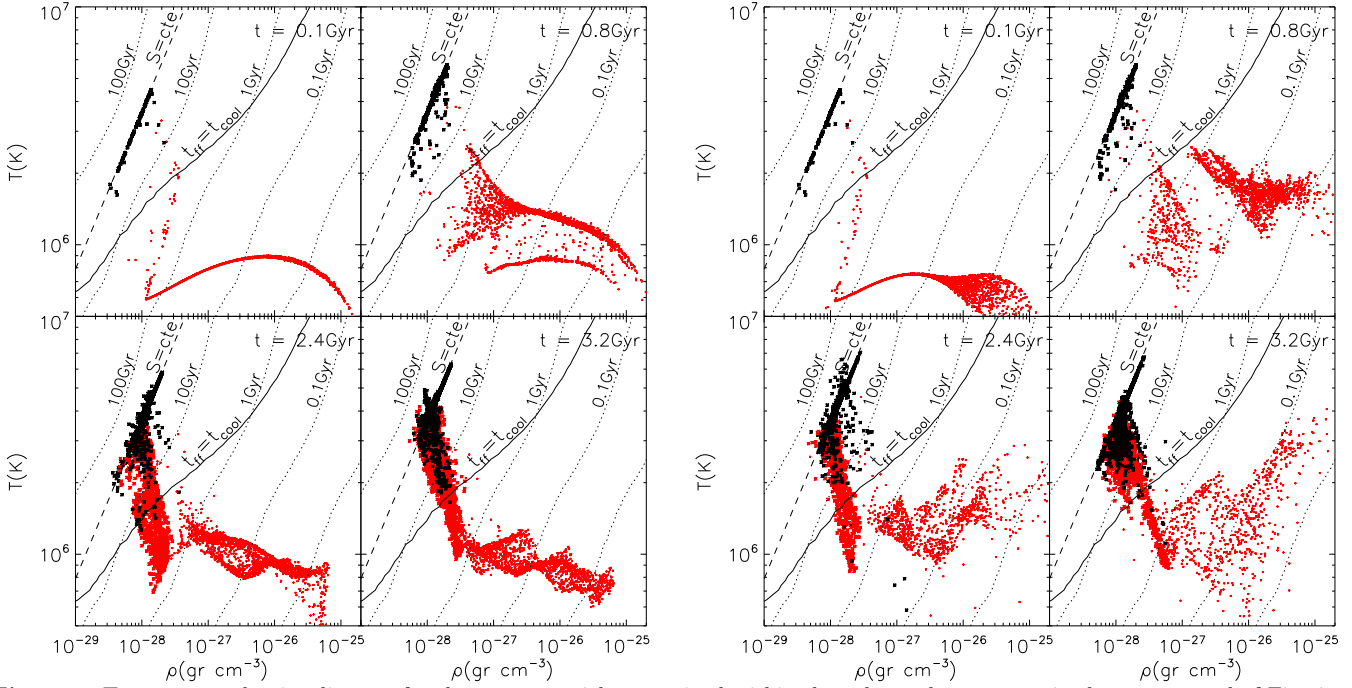


Figure 5. Temperature-density diagram for the tracer particles contained within the volume that appears in the upper panel of Fig. 4. Only a random subsample of the full tracer population within this region is plotted (except in the bottom panels for the region around the wakes, $X > 500$ kpc in Fig. 2, where the tracers are shown with bigger symbols). The red (black) points are for the satellite (ICM). The simulation times shown are $t = 0.1, 0.8, 2.4$ and 3.2 Gyr. The dotted lines are lines of constant cooling time (assuming $\log_{10}(Z/Z_{\odot}) = -0.5$) and the black solid line shows the locus of points where $t_{\text{ff}} = t_{\text{cool}}$. The dashed lines mark an example of a path with constant entropy. The set of panels to the left (right) corresponds to the simulation without (with) radiative cooling.

the mass that is no longer bound to the satellite is in the trailing wakes in the simulations with and without radiative cooling, respectively. In the former the amount of stripped gas is $\sim 7 \times 10^9 M_{\odot}$, a factor of 3 smaller than in the latter.

The gas in the ICM mixes with the gas from the satellite and becomes part of the trailing wakes. Although this mixing occurs in a wide region, we can arbitrarily define the “warm phase” as the region in the wakes where the gas (both from the ICM and from the satellite) has an entropy which is at least 50% lower than the initial entropy of the ICM. Gas with higher entropy has either not been thoroughly mixed yet and/or contains the highest entropy gas from the satellite. Using this definition, we can narrow down the median values of the temperature and density of the gas that is more likely to cool afterwards and estimate its total mass after 3.2 Gyr of the evolution for the simulation without (with) radiative cooling: $\langle T_{\text{mix}} \rangle \sim 2(2.1) \times 10^6 \text{ K}$, $\langle \rho_{\text{mix}} \rangle = 1.8(1.8) \times 10^{-28} \text{ g cm}^{-3}$, and $M_{\text{mix}} = 7.6(1.4) \times 10^9 M_{\odot}$ ($\sim 20(28)\%$ coming from the ICM). These values imply $t_{\text{cool}} \sim 7(8) \text{ Gyr}$, a factor of $\sim 6(5)$ less than that of the ambient ICM. In the non-radiative simulation, most of the gas in the wakes that came from the satellite belongs to the warm phase (59%), while in the dissipative simulation is a minority (27%). This is simply explained by the smaller amount of stripped gas that participates in the mixing in the dissipative simulation, which also explains why the warm phase has a longer cooling time in this case.

5 DISCUSSION

The relatively weak impact of radiative cooling in the formation and initial properties of the wakes (with the main difference being a reduction of the stripped gas) can be understood by noting the following. The gas in the satellite that participates in the mixing is given, at the most, by the gas within a shell external to the stripping radius. Even if all the gas within this radius were to collapse immediately due to radiative losses, the outer shell would collapse in a free-fall time, which is $\gtrsim 1$ Gyr; this contraction would happen adiabatically since the gas in the shell has still quite a long cooling time. An adiabatic process preserves the cooling time at the temperatures and densities of the collapsing shell (note how the lines of constant entropy are roughly parallel to the lines of constant cooling time in Fig. 5). This is because the cooling function goes as $\Lambda_{\text{cool}} \propto T^{-\alpha}$, with $\alpha \sim 0.5$ for $\log_{10}(Z/Z_{\odot}) \sim -0.5$, in the temperature range between 10^5 K and $\sim 5 \times 10^6 \text{ K}$. Thus, the gas in the shell, that is eventually stripped, has enough time to mix with the ICM forming a wake in a qualitatively similar way as in the non-radiative simulation.

In detail, the properties of the wakes depend on the evolutionary stage of the interaction and, of course, on the metallicity, temperature and density of the gas being stripped. The latter depend on the assumed radial profiles and have important consequences in our results. Although we cannot check directly from observations if these profiles are adequate, we found that the the properties of the gas near the outskirts of the corona are roughly the same as the ones reported in Crain et al. (2010) (based on a large

sample of MW-size galaxies extracted from a cosmological simulation). The mass of stripped gas not only depends on the balance of radiative cooling and central feedback (which determines how fast the central collapse relative to the stripping time scale is) but also in the uncertain amount of hot gas that is in the corona. In this work we have used the largest possible value set by the universal baryon fraction. However, e.g. Anderson & Bregman (2010, 2011) found that the actual amount of mass in the hot coronae is considerably less than naively expected from subtracting the universal baryon fraction from the amount of baryons that is locked in stars and cold gas. A lower gas fraction would lower the mass of stripped gas. Because of all this, our predictions cannot be made in terms of the absolute values of the properties of the gas that mixes, but rather in terms of the mixed gas fraction relative to the stripped gas, and its cooling efficiency relative to the temperature and density of the removed gas.

Our non-radiative simulation indicates that the analytic model we introduced in Section 2 gives reasonable estimates. In particular, once we apply the model to the conditions in the simulation, we find that it is able to reproduce some of the global properties of the wakes (see below) once we adjust its parameters and add two additional components to it: i) The stripped gas is shock-heated to temperatures in excess of the virial temperature of the satellite before it mixes with the ICM. We can account for this effect by calculating the Rankine-Hugoniot (RH) temperature jump conditions of the shock (leading to a shock-heated temperature $\sim 1.7 \times 10^6$ K); ii) The gas in the wakes is compressed by a factor δ_{mix} relative to the density of the ICM. With these considerations we find that by taking: $\alpha_{\text{rem}} \sim 1$, $\beta \sim 3$, and $\delta_{\text{mix}} \sim 2$ we are able to reproduce the amount of stripped gas, the median temperature in the mixed phase and its cooling time. Although comparing the analytical model to the dissipative simulation is in principle more complicated due to the contraction of the corona, it is possible to use the current model without modifications if we assume that the contraction occurs rapidly relative to the gas removal processes. Then, the results of the dissipative simulation can be matched by setting $\alpha_{\text{rem}} = 1/3$ and $\beta = 1.5$. The first of these parameters is reduced, relative to the non-radiative case, to accommodate a smaller amount of stripped gas, while the second is reduced since the corona is more compact.

Perhaps the most important limitation of the model arises from the complex nature of the mixing process which occurs in the turbulent eddies in layers of different size. This implies that defining an overall effective value for β is unrealistic since there is a broad distribution of cross sectional areas. In the simulations, the mixing happens along the annulus formed by the wake, which has a cross sectional area that broadens if the relative velocity of the satellite decreases. Although the gravitational focusing effect is stronger in this case, the gas in the turbulent eddies is confined to a region which is more extended than the case of larger velocity since the ram pressure of the surrounding ICM is smaller (we have corroborated this by running an identical simulation but with $v_{\text{sat}} = 150 \text{ km/s}$). This suggests that β increases (decreases) for lower (higher) velocities, contrary to expectations.

Despite its simplicity, the analytic model could be used for instance in semi-analytic models (SAMs) of galaxy for-

mation (for a review see e.g. Baugh 2006) to account for the removal processes of the coronal gas, which are typically severely simplified by assuming that this gas is removed instantaneously having no further importance.

There are specific conditions one can think of that would enhance the mechanism proposed in this work. For instance, if the infalling satellite has lower mass and hence a colder corona, the temperature in the mixture would be lower than the case we analysed, and gas removal would be more efficient. A lower infall velocity would create a weaker shock and thus a reduction on the temperature of the shock-heated gas as it is stripped from the satellite⁷. On the other hand, the strength and time scale of gas removal decrease making the mixing process less efficient.

Although more speculative, we also expect that the mechanism would be more important as the satellite spirals towards the centre of the dense stratified medium of the host. We can crudely estimate what would happen in these circumstances using our analytic model. Although the process is of course gradual, let's assume that by the time the satellite is at a distance of $0.5r_{\text{v,host}}$ from the centre of the host, it has lost an amount of dark matter and gas as predicted by the analytic estimates at the virial radius, i.e., the satellite arrives at this orbital distance with a mass profile “clipped” at a tidal stripping radius $r_t = 0.65r_v$ (see Table 2). If the specific angular momentum of the satellite was conserved along its orbit, then its velocity would be twice the velocity at the virial radius. Dynamical friction however, decelerates the satellite; for simplicity we assume it to be $\sim 1.5v_{\text{sat}}$ ⁸. The temperature in the corona of the satellite is that left by the remnant of the initial shock, which is given by the RH jump conditions of the virial shock. The temperature and density of the ICM at this position are $3.5 \times 10^6 \text{ K}$ and $6 \times 10^{-28} \text{ g cm}^{-3}$, respectively. Under these conditions, we applied our analytic method and find that the remaining corona would be removed in a time scale roughly given by the sound crossing time $\lesssim 1 \text{ Gyr}$, and the gas in the mixture would have a cooling time of only 1.5 Gyr (a factor of ~ 4 less than the ambient ICM).

It is worth mentioning that recent hydrodynamical simulations of galaxy formation performed with the code AREPO (Springel 2010a, a hybrid method combining some of the advantages of Lagrangian and Eulerian codes and avoiding their most important weaknesses) have reported significantly higher star formation rates for central galaxies in massive haloes than the ones found, under the same conditions, in an SPH formulation (Keres et al. 2011). The authors advocate that the difference is partly due to a more

⁷ The typical satellite infall velocities are of the order of the virial velocity of the group, lower infall velocities are nevertheless possible (e.g. Wetzel 2011). For example, if $v_{\text{sat}} = 150 \text{ km/s}$, then the temperature ratio of the post- to pre-shock gas according to the RH temperature jump conditions is reduced from 2.8, in the case when $v_{\text{sat}} = 315 \text{ km/s}$, to 1.6.

⁸ We ran a dark-matter only simulation of a MW-size halo merging with a $10^{13} M_{\odot}$ group. The initial infall velocity of the satellite, with its radial and tangential components, was set to the average value as given in Wetzel (2011). We found that the satellite reaches an orbital distance of $0.5r_{\text{v,host}}$ with a speed of $\sim 1.6v_{\text{sat}}$ with approximately 70% of its original dark matter mass. This simulation confirms the orbital evolution we have assumed here.

efficient mixing in AREPO, caused by a larger removal of low entropy material from infalling satellites (Vogelsberger et al. 2011). Fig. 4 of Keres et al. (2011) shows that for a $\sim 10^{13} M_{\odot}$ halo at the present day, this difference is a factor of ~ 2 : AREPO predicts approximately $3 \times 10^{11} M_{\odot}$ of additional stars. It is unlikely that the majority of this extra mass can be accounted for by the coronae mixing studied in this paper, however it might be that a significant portion of the additional star formation material comes from a similar mixing process between the ICM and the cold gaseous disc of the merging galaxy. We believe it would be interesting to explore the relative contribution of both of these processes.

6 CONCLUSIONS

The presence of an extended corona of hot gas within clusters, groups and massive galaxies is a generic prediction of the current theory of galaxy formation. Since such coronae are a large gas reservoir that can potentially cool down and form stars, it is of great relevance to study their evolution and in particular their interaction during galaxy mergers which are ubiquitous in the CDM paradigm.

Most studies of galaxy mergers have concentrated on the interaction of the cold components (stars and gaseous discs), relegating the hot coronae to a secondary role essentially governed by ram pressure stripping. In the case of MW-size galaxies merging into groups, the high temperature and low density of the ambient ICM at the outskirts of the groups are commonly assumed to imply that the stripped gas stays irrelevant for subsequent cooling and star formation. This assumption, however, ignores the fact that Kelvin-Helmholtz instabilities produced by the velocity shear also remove coronal gas and efficiently mix it with the ICM through turbulent eddies. Since the former is colder than the latter, the mixture could have a shorter cooling time than the ambient intragroup gas. These instabilities are typically suppressed in the majority of galaxy formation simulations that have been done to date since most of them were carried out using the SPH formulation (Agertz et al. 2007).

In this paper, we use analytic methods and hydrodynamical simulations (with and without radiative cooling) to study the gas removal processes that act during the interaction of a spherical MW-size corona moving through a homogeneous ICM wind representative of the coronal gas at the virial radius of a low-mass group. The main conclusions of our work are the following:

- Our simulations show that a relevant fraction of the removed coronal gas mixes with the ICM in trailing wakes creating a “warm phase” (i.e. with at least 50% less entropy than the ambient ICM) with a cooling time which is almost an order of magnitude lower than the cooling time of the ambient intragroup gas. This reduction is a result of a lower temperature in the gas mixture driven by the colder coronal gas from the satellite, as anticipated, but also due to an enhanced density caused by compression.
- We find that the gas mass in this warm phase is between 40-76% of the mass stripped from the satellite and deposited in the wakes ($M_{\text{warm}} \sim 1.4 - 7.6 \times 10^9 M_{\odot}$ for the parameters we have used in our simulations). This gas is mostly com-

ing from the satellite, but a non-negligible fraction, 20-28%, comes from the ICM.

- The analytic model described in Section 2 is able to roughly estimate the amount of removed mass and the time scale of removal due to the two main acting mechanisms: ram pressure stripping and KH instabilities. Moreover, once properly calibrated, it can be used to estimate the most likely temperature and cooling time of the gas mixture after the gas settles in the turbulent wakes. We believe that this model can be incorporated into semi-analytic models of galaxy formation to account for these processes, which are typically ignored in current implementations.

We speculate that the warm phase created through the mechanism proposed in this work has the potential to become a mode of star formation in galaxy groups (through in situ star formation and/or through a cold stream flowing to the central galaxy of the host). In fact, the possibility of stars forming in turbulent wakes from the condensation of gas stripped from cold discs seems to be a likely hypothesis in some observed cases (e.g. Hester et al. 2010). Although in such cases the mechanism at work is the same we have studied here, star formation is far more likely in those since the gas being removed is much colder than the ambient gas. We are thus cautious in speculating about the fate of the removed coronal gas. In particular, it is not clear whether the gas mixture can survive long enough without evaporating through conduction with the ICM (e.g. Nipoti & Binney 2004). This would depend on the specific details of conduction in the surfaces of the turbulent wake, which are difficult to estimate. It is therefore crucial to address these questions using more detailed simulations. We believe that the results of this work motivate further analyses to fully quantify the effect of the mixing of the coronal gas from satellites with the intragroup gas.

ACKNOWLEDGMENTS

We thank the anonymous referee for helpful suggestions. We thank John ZuHone for helpful comments on the simulation setup with FLASH. We acknowledge David Gilbank and Ting Lu for helpful conversations during the early stages of this work, and Volker Springel and Mark Vogelsberger for helpful discussions towards the completion of this paper. NA wishes to thank David Spergel for helpful discussions. JZ and NA are supported by the University of Waterloo and the Perimeter Institute for Theoretical Physics. Research at Perimeter Institute is supported by the Government of Canada through Industry Canada and by the Province of Ontario through the Ministry of Research & Innovation. JZ acknowledges financial support by a CITA National Fellowship. MLB acknowledges a NSERC Discovery Grant. This work was made possible by the facilities of the Shared Hierarchical Academic Research Computing Network (SHARC-NET:www.sharcnet.ca) and Compute/Calcul Canada.

APPENDIX A: RPS TIME SCALE

The properties of the initial shock generated by the colliding coronae and the values of the post-shock thermodynamic variables can be estimated by solving a one-dimensional

shock tube problem. Once the shock develops, let region 1 to the left be the unperturbed ICM moving to the right with a relative velocity v_{sat} and with properties $(\rho, P, u, c_s)_1 = (\rho_{\text{host}}, P_{\text{host}}, v_{\text{sat}}, c_{s,\text{host}})$, and region 4 to the right be the unperturbed corona of the satellite at rest having properties: $(\rho, P, u, c_s)_4 = (\rho_{\text{sat}}(r_v), P_{\text{sat}}(r_v), 0, c_{s,\text{sat}}(r_v))$. Regions 1 to 4 separate the three *characteristics* of the problem. The forward shock front divides regions 3 and 4; thus, region 3 contains the post-shock material. The solution to this problem is found by solving the following transcendental equation:

$$\frac{P_1}{P_4} = 1 = \xi \left[1 + \frac{\gamma - 1}{c_{s,1}} \left(u_1 - \frac{c_{s,4}}{2\gamma} \frac{\xi - 1}{\sqrt{\lambda(\xi - 1) + 1}} \right) \right]^{-2\gamma/(\gamma-1)}, \quad (\text{A1})$$

where $\xi = P_3/P_4$ and $\lambda = (\gamma + 1)/2\gamma$, and we have assumed that the corona of the satellite and the ICM are in pressure equilibrium at first: $P_1/P_4 = 1$. The velocity of the shock, and the velocity of the post-shock fluid are then given by:

$$\begin{aligned} v_{\text{sh}} &= c_{s,4} \sqrt{\lambda(\xi - 1) + 1}, \\ v_{\text{ps}} &= c_{s,4} \frac{(\xi - 1)}{\gamma \sqrt{\lambda(\xi - 1) + 1}}. \end{aligned} \quad (\text{A2})$$

Once the shock is generated it will propagate towards the centre of the satellite. The density stratification of the latter will then change the speed of the shock and modify the post-shock properties of the newly encountered material. To roughly estimate the propagation of the shock, we follow the description of Kogure & Osaki (1962) that reduces the evolution of the post- and pre-shock pressure ratio ξ to the following ordinary differential equation (derived from a one-dimensional problem neglecting the effects of gravity and radiative losses, see their Eq. 3.1):

$$\begin{aligned} \frac{d\xi}{ds'} &= - \frac{(1 + \xi)(1 + \lambda\xi)(2 + (3 - \lambda)\xi)}{4 + 2(2 + \lambda)\xi + \lambda(3 - \lambda)\xi^2} \frac{d \ln P}{ds'} \\ &+ \frac{\xi(1 + \xi)(1 + \lambda\xi)}{4 + 2(2 + \lambda)\xi + \lambda(3 - \lambda)\xi^2} \frac{d \ln \rho}{ds'}, \end{aligned} \quad (\text{A3})$$

where s' is the Lagrange coordinate of the shock front. In reference to the variable $s = r/r_v$ from the centre of the satellite in Eqs. (1) and (3), $s' = 1 - s$. Thus, solving Eq. (A1) assuming pressure equilibrium in the boundary we get $\xi(s' = 0) = 9.0(12.9)$ for the galaxy-group (galaxy-cluster) interaction. With this boundary condition, we can solve Eq. (A3) to find $\xi(s')$ and use it in the first of Eqs. (A2) to get the shock speed as a function of s' , which can then be substituted in Eq. (5) to find the time scale for RPS.

REFERENCES

Agertz O., Moore B., Stadel J., Potter D., Miniati F., Read J., Mayer L., Gawryszczak A., Kravtsov A., Nordlund Å., Pearce F., Quilis V., Rudd D., Springel V., Stone J., Tasker E., Teyssier R., Wadsley J., Walder R., 2007, *MNRAS*, 380, 963
 Anderson M. E., Bregman J. N., 2010, *ApJ*, 714, 320
 Anderson M. E., Bregman J. N., 2011, *ApJ*, 737, 22
 Bauer A., Springel V., 2012, *MNRAS*, 423, 2558
 Baugh C. M., 2006, *Reports on Progress in Physics*, 69, 3101

Binney J., Nipoti C., Fraternali F., 2009, *MNRAS*, 397, 1804
 Binney J., Tremaine S., 1987, *Galactic dynamics*
 Borgani S., Murante G., Springel V., Diaferio A., Dolag K., Moscardini L., Tormen G., Tornatore L., Tozzi P., 2004, *MNRAS*, 348, 1078
 Boylan-Kolchin M., Bullock J. S., Kaplinghat M., 2012, *MNRAS*, 422, 1203
 Boylan-Kolchin M., Ma C.-P., Quataert E., 2008, *MNRAS*, 383, 93
 Chandrasekhar S., 1943, *ApJ*, 97, 255
 Ciotti L., Ostriker J. P., 1997, *ApJ*, 487, L105
 Colella P., Woodward P. R., 1984, *Journal of Computational Physics*, 54, 174
 Cowie L. L., McKee C. F., 1977, *ApJ*, 211, 135
 Crain R. A., McCarthy I. G., Frenk C. S., Theuns T., Schaye J., 2010, *MNRAS*, 407, 1403
 Dai X., Anderson M. E., Bregman J. N., Miller J. M., 2012, *ApJ*, 755, 107
 Diemand J., Kuhlen M., Madau P., 2007, *ApJ*, 667, 859
 Drazin P. G., Reid W. H., 1981, *NASA STI/Recon Technical Report A*, 821, 17950
 Fakhouri O., Ma C.-P., Boylan-Kolchin M., 2010, *MNRAS*, 406, 2267
 Fryxell B., Olson K., Ricker P., Timmes F. X., Zingale M., Lamb D. Q., MacNeice P., Rosner R., Truran J. W., Tufo H., 2000, *ApJS*, 131, 273
 Fukugita M., Peebles P. J. E., 2004, *ApJ*, 616, 643
 Fukugita M., Peebles P. J. E., 2006, *ApJ*, 639, 590
 Gan J., Kang X., van den Bosch F. C., Hou J., 2010, *MNRAS*, 408, 2201
 Gao L., Navarro J. F., Cole S., Frenk C. S., White S. D. M., Springel V., Jenkins A., Neto A. F., 2008, *MNRAS*, 387, 536
 Gnat O., Sternberg A., 2007, *ApJS*, 168, 213
 Gunn J. E., Gott III J. R., 1972, *ApJ*, 176, 1
 Heinz S., Churazov E., Forman W., Jones C., Briel U. G., 2003, *MNRAS*, 346, 13
 Heitsch F., Putman M. E., 2009, *ApJ*, 698, 1485
 Hester J. A., Seibert M., Neill J. D., Wyder T. K., Gil de Paz A., Madore B. F., Martin D. C., Schiminovich D., Rich R. M., 2010, *ApJ*, 716, L14
 Kazantzidis S., Magorrian J., Moore B., 2004, *ApJ*, 601, 37
 Keres D., Vogelsberger M., Sijacki D., Springel V., Hernquist L., 2011, *ArXiv e-prints*
 Kogure T., Osaki T., 1962, *PASJ*, 14, 254
 Li Z., Wang Q. D., Hameed S., 2007, *MNRAS*, 376, 960
 Malagoli A., Bodo G., Rosner R., 1996, *ApJ*, 456, 708
 Marinacci F., Binney J., Fraternali F., Nipoti C., Ciotti L., Londrillo P., 2010, *MNRAS*, 404, 1464
 Mathews W. G., Brighenti F., 1998, *ApJ*, 503, L15
 Mathews W. G., Brighenti F., 2003, *ARA&A*, 41, 191
 McCarthy I. G., Frenk C. S., Font A. S., Lacey C. G., Bower R. G., Mitchell N. L., Balogh M. L., Theuns T., 2008, *MNRAS*, 383, 593
 Mitchell N. L., McCarthy I. G., Bower R. G., Theuns T., Crain R. A., 2009, *MNRAS*, 395, 180
 Mo H., van den Bosch F. C., White S., 2010, *Galaxy Formation and Evolution*
 Mori M., Burkert A., 2000, *ApJ*, 538, 559
 Moster B. P., Macciò A. V., Somerville R. S., Naab T., Cox T. J., 2011, *MNRAS*, 415, 3750

- Murray S. D., White S. D. M., Blondin J. M., Lin D. N. C., 1993, *ApJ*, 407, 588
- Navarro J. F., Frenk C. S., White S. D. M., 1996, *ApJ*, 462, 563
- Navarro J. F., Frenk C. S., White S. D. M., 1997, *ApJ*, 490, 493
- Neto A. F., Gao L., Bett P., Cole S., Navarro J. F., Frenk C. S., White S. D. M., Springel V., Jenkins A., 2007, *MNRAS*, 381, 1450
- Nipoti C., 2010, *MNRAS*, 406, 247
- Nipoti C., Binney J., 2004, *MNRAS*, 349, 1509
- Nulsen P. E. J., 1982, *MNRAS*, 198, 1007
- Rasmussen J., Ponman T. J., 2009, *MNRAS*, 399, 239
- Ricker P. M., 2008, *ApJS*, 176, 293
- Sakellou I., 2000, *MNRAS*, 318, 1164
- Spitzer L., 1956, *Physics of Fully Ionized Gases*
- Springel V., 2010a, *MNRAS*, 401, 791
- Springel V., 2010b, *ARA&A*, 48, 391
- Springel V., Wang J., Vogelsberger M., Ludlow A., Jenkins A., Helmi A., Navarro J. F., Frenk C. S., White S. D. M., 2008, *MNRAS*, 391, 1685
- Springel V., White S. D. M., Jenkins A., Frenk C. S., Yoshida N., Gao L., Navarro J., Thacker R., Croton D., Helly J., Peacock J. A., Cole S., Thomas P., Couchman H., Evrard A., Colberg J., Pearce F., 2005, *Nature*, 435, 629
- Stevens I. R., Acreman D. M., Ponman T. J., 1999, *MNRAS*, 310, 663
- Sun M., Donahue M., Roediger E., Nulsen P. E. J., Voit G. M., Sarazin C., Forman W., Jones C., 2010, *ApJ*, 708, 946
- Taylor J. E., Babul A., 2001, *ApJ*, 559, 716
- van de Voort F., Schaye J., 2012, *MNRAS*, p. 2882
- Vietri M., Ferrara A., Miniati F., 1997, *ApJ*, 483, 262
- Vikhlinin A., Kravtsov A., Forman W., Jones C., Markevitch M., Murray S. S., Van Speybroeck L., 2006, *ApJ*, 640, 691
- Vikhlinin A., Markevitch M., Murray S. S., Jones C., Forman W., Van Speybroeck L., 2005, *ApJ*, 628, 655
- Vogelsberger M., Sijacki D., Keres D., Springel V., Hernquist L., 2011, *ArXiv e-prints*
- von Neumann J., 1951, *National Bureau of Standards Applied Mathematics Series*, 12, 36
- Wetzel A. R., 2011, *MNRAS*, 412, 49
- White S. D. M., Frenk C. S., 1991, *ApJ*, 379, 52
- White S. D. M., Rees M. J., 1978, *MNRAS*, 183, 341
- Zentner A. R., Berlind A. A., Bullock J. S., Kravtsov A. V., Wechsler R. H., 2005, *ApJ*, 624, 505